Heliyon 7 (2021) e07019

Contents lists available at ScienceDirect

Heliyon

journal homepage: www.cell.com/heliyon

Research article

Development of solar cell for large area position detection: proof of concept

Heba Abdelmoneim [a], Abdelhalim Zekry [a], Ahmed Shaker [b,*]

[a] Department of Electronics and Communications, Faculty of Engineering, Ain Shams University, Cairo, Egypt
[b] Department of Engineering Physics and Mathematics, Faculty of Engineering, Ain Shams University, Cairo, Egypt

ARTICLE INFO

Keywords:
Solar cell
Large active area motion detector
Position sensitive detector
PSD
Output display
TCAD
Simulation
Position detection error

ABSTRACT

Detecting and analyzing a moving body position are helpful in many fields, such as medicine, sports performance, virtual reality and many more. Therefore, researchers try to develop a tool or a system that helps to detect the motion and tracking its position. This paper shows how a Si solar cell can be modified to function as a Position Sensitive Detector (PSD), which could be used as a large area detector in a position detection system. To develop the new detector, we modeled and simulated the modified solar cell by TCAD simulation tools to calculate the detected photocurrent as a function of the position of an incident laser beam sourced by the moving object. Further, an optical position detection system is implemented containing the modified solar cell, a signal amplifier and a microcontroller. The output is then displayed on a Laptop. By measuring the same simulated output photocurrents, it is found that the measured system output matches the simulation results. This proposed position detection system is relatively cheap because it does not contain high precision optical image building components such as lenses and mirrors. Besides, the proposed system could substitute the optical system by using a large area PSD made from a broad array of solar cells. The electronics are also much more straightforward than those in systems based on image processing. So, it has a high-speed response. The error assessment of the proposed system showed a low position detection error of less than 10%.

1. Introduction

The motion detection of a moving body is a research point that gained significant interest because of its various applications in different fields ranging from automatic video surveillance [1], rehabilitation [2], athletics [3], computer graphics [4] to other applications. A lot of motion detection systems have been proposed using different devices [5, 6] and technologies such as systems based on image processing using video cameras [7], accelerometers and gyroscopes [8], microwave sensor module utilizing Doppler shift frequency principle [9] or multi-beam passive infrared sensor [10].

The Position Sensitive Detector (PSD) is a sensor that can track a laser beam moving on its surface. It could detect the laser position in 1D or 2D where the output current gives the incident light spot position. The PSDs are used in many applications such as: determining the location, energy loss, the occurrence time of single ionizing events [11], rotational speed measurement [12], atom probe microanalysis [13], the micro-robotic applications [14], measurement of atmospheric turbulence [15] and noncontact vibration measurement [16]. Besides, a PSD can work as a position detector on a large scale, but in this case, it needs an optical imaging subsystem, which is usually very expensive and needs a very careful calibration. Attempts to build such a large area motion detection system using large convex mirrors and concave lenses are studied in [17].

A better solution to this problem is to construct a large area PSD using modified solar cells. Solar cells are optimized for light detection, and they are large area devices with very affordable cost. So, one can directly let the laser beam attached to the moving object strike the PSD-like solar cell.

In this paper, we introduce a novel technique to detect the moving body position by taking advantage of the common characteristics shared by the PSD and the solar cell to develop a solar cell that can function as a position detector. Then, processing the output signal of this modified solar cell using a microcontroller circuit is performed. Furthermore, the output is displayed using a PC application. The combination of the useful features of both the solar cell and the PSD achieves some advantages. Regarding the solar cell, the benefits include its large active area compared to the PSD active area, low price and availability. For the PSD, the advantages include its high-speed response, excellent position resolution and wide-spread response range.

* Corresponding author.
E-mail address: ahmed.shaker@eng.asu.edu.eg (A. Shaker).

https://doi.org/10.1016/j.heliyon.2021.e07019
Received 31 October 2020; Received in revised form 30 January 2021; Accepted 5 May 2021

The rest of the paper is arranged as follows. Section II includes an illustration of the basic principles of the PSDs and the solar cells as well as the standard features between them. Section III consists of a simulation analysis carried out by using SILVACO TCAD device simulator [18, 19, 20] followed by the process to achieve the proposed motion detection system. Then, the system's final results and the calculations of the position detection error are presented, which are performed utilizing an application that has been developed using C# Graphical User Interface (GUI) class library [21] and the ZedGraph class library [22].

2. The system basic theory

Solar cell and PSD are considered as a simple p-n junction with the photovoltaic effect as the common detection principle between them, where a solar cell represents an unbiased photodiode [23, 24]. By contrast, a PSD represents a reverse-biased photodiode. A PSD consists of a resistive layer formed on a high-resistivity substrate on one or both sides of its surface. A pair of electrodes for extracting the position signals is formed on both ends of the resistive layer. The photosensitive area has a p-n junction that generates photocurrent employing the photovoltaic effect [19]. When a laser beam is incident on the active area of the PSD, an electric charge is generated producing a current that is proportional to the light intensity. This current is pushed through the top resistive layer and then, collected by the output electrodes, where the two output current signals are inversely proportional to the distance between each electrode and the light spot position [25].

Figure 1 represents a schematic view of a PSD cross-section showing the operating principle. A resistive layer of p-type is formed on an n-type high-resistivity silicon substrate with two electrodes on its both ends. This resistive layer serves as a photosensitive area for photoelectric conversion. An electrode is formed below the whole backside of the silicon substrate. It is the same structure as that of PIN photodiodes with its p-type top layer acting as the resistive layer on the surface through which the photocurrent is collected [25].

The relation between the position of the incident light spot and the output currents from the electrodes depends on the point that will be considered as the origin. It could be a case of the following two. When the origin is set at the center point of PSD then,

$$\frac{I_{X2}-I_{X1}}{I_{X1}+I_{X2}}=\frac{2X_A}{L_X} \tag{1}$$

And when the origin is set at the end of PSD,

$$\frac{I_{X2}-I_{X1}}{I_{X1}+I_{X2}}=\frac{2X_B-L_X}{L_X} \tag{2}$$

where I_{X1} is electrode X1 output current; I_{X2} is electrode X2 output current; X_A is the distance from the light spot to the center of the PSD; X_B is the distance from the light spot to the electrode X1; L_X is the resistance length.

Further, Figure 2 shows the main features of the crystalline silicon (c-Si) solar cell. The absorber material is a moderately doped p-type wafer. A highly doped n^+-type layer is formed on the top side of the wafer. This n-p junction is sandwiched between a full metal back and partially front metal electrodes where metal fingers are placed on the solar cell surface. Silicon solar cells have typical thicknesses in between 100 and 300 μm. When the solar cell is illuminated with sunlight, the photons are converted to charge carriers (electrons and holes). These charge carriers will be separated to conductive contacts to transmit the generated voltage [19, 26, 27].

As illustrated, the characteristics of the PSD and the solar cell are considered p-n junction photodiodes. According to that and by applying some modifications to the solar cell surface, it could work as a PSD.

3. Results and discussions

3.1. TCAD simulation

To demonstrate the concept of converting a solar cell to a PSD, a 2D simulation analysis is performed like REF [28]. In our work, the simulation analysis of the modified solar cell is utilized using a process simulator Athena and device simulator Atlas provided by SILVACO TCAD. The simulation consists of two parts. The first part is defining the structure of the modified solar cell, which is done by using the process simulator Athena as follows. Firstly, a p-type substrate is initialized, and then an implementation of the n^+ layer is done. Next, the aluminum deposition is performed, followed by electrodes formation using etching. Table 1 shows the parameters used in this part. The second part is executed by using the device simulator Atlas by providing the light source file and its position on the modified solar cell. After that, the biasing conditions are determined and finally, the output current, associated with these biasing conditions, is extracted.

Table 1. The used parameters in the Athena process simulation.

Structure parameter	Value
Base (P layer) doping	10^{14} cm^{-3}
n+ layer doping	10^{15} cm^{-3}
Solar cell thickness	50 μm
Solar cell width	100 μm
Oxide thickness	0.05 μm
Cathodes thickness	0.1 μm
Cathodes width	5 μm

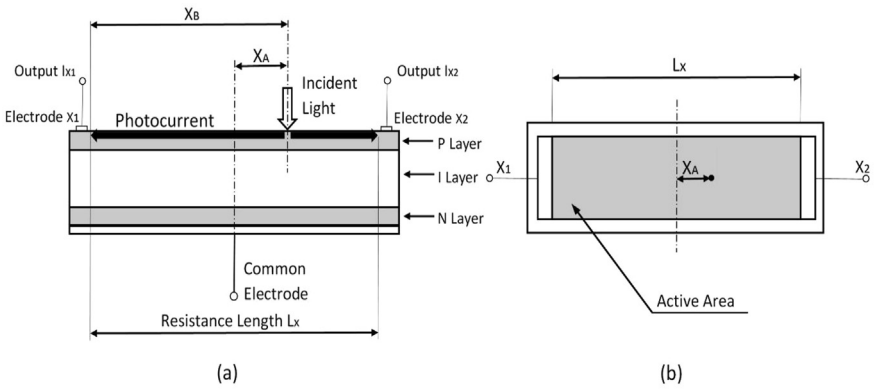

Figure 1. (a) PSD cross-sectional view and (b) Active Area (plan view).

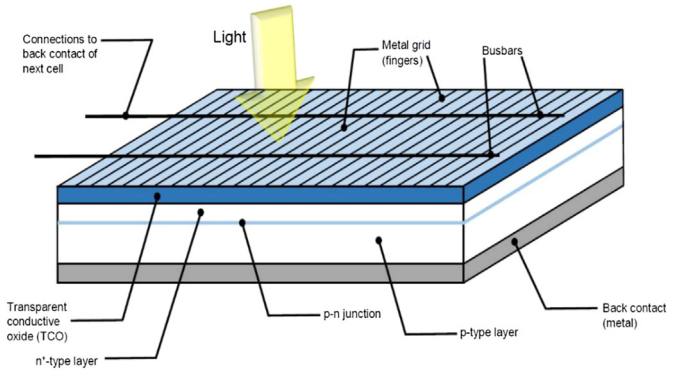

Figure 2. The solar cell schematic diagram.

In this simulation part, the light absorption and photogeneration rates in the device are obtained using geometric ray tracing. This step is followed by an electrical simulation to calculate the required terminal currents. The main physical models are enabled. Regarding mobility, a concentration-dependent and field-dependent mobility models are incorporated. Further, concentration-dependent Shockley–Read–Hall (SRH) and Auger recombination mechanisms are invoked. The electron and hole lifetimes are taken to be equal and set to 1 μs.

Figure 3 shows a cross-section view of the modified solar cell with a total length of 100 μm and two cathodes with a width of 5 μm; each of which provides an active area of length 90 μm. It should be pointed out here that the real device with much larger dimensions is scaled down to save calculation time while proving the concept of the operation presented in the previous section.

Now, the device structure is subjected to a laser beam source to study its impact on the device behavior. In this regard, Figure 4 illustrates the photogeneration rate at the points where the laser beam of a wavelength of 650 nm falls and the total current density corresponds to it. The figures were taken at different points at -20, 0 and 40 μm to show how the output current changes with the laser position. The output current of the electrode closer to the position where the laser beam fall has a higher value than the current of the other electrode.

The simulation is performed by sweeping the laser beam across the sensor active area total length and recording the values of the output currents at 25 positions. Accordingly, a graph that represents the relation between the output currents and the laser beam position is drawn. Figure 5(a) shows the plot of the simulated output currents I_1 and I_2 while using two laser beams with different wavelengths one with a wavelength of 650 nm and the other with a wavelength of 532 nm versus the horizontal position X of the light spot. It is clear that I_1 decreases with X while I_2 increases. This is because the scanning with a light beam starts from left near cathode 1. The simulation output matches well with the results expected from a PSD. The difference between the cathode currents $I_2 - I_1$ is plotted in Figure 5(b). We can see that the difference between the cathode currents follows a straight line whose equation can be formulated as follows:

$$X = \frac{L_x}{2}\left(\frac{I_2 - I_1}{I_1 + I_2}\right) \tag{3}$$

where L_x is the active area length. This relation agrees with that given in Eq. (1).

3.2. The proposed motion detection system realization

A schematic diagram of the proposed motion detection system is depicted in Figure 6. The moving system contains a laser source fixed on the moving part. The laser beam is received and detected by the new solar cell detector. Also, the detected signal is amplified by a signal amplifier, converted into digital form with an A/D converter and finally, the signal is plotted by an output display. Figure 6 shows the equivalent circuit of the modified solar cell detector and the amplifiers drawn by using a Proteus design software [29]. The solar cell detector is represented by a distributed network [30]. The system components are described as follows (see Figure 7).

3.2.1. Laser

The Laser unique features [31] make it suitable to be used as the indicator of the moving body position in our system.

3.2.2. The modified solar cell position detector

The solar cell modification is the focus of this research since it could work as the detector of the moving body position. As explained therebefore, a mapping between the PSD and the solar cell is needed to achieve our target. Figure 8 shows the front and back of the solar cell (Crystalline silicon type with thickness of 250 μm consisting of N-type front layer and P-type back layer); the surface layer of the solar cell consists of two types of contacts, namely the busbars that conduct the electric power generated by the cell and the cell fingers that collect the generated DC and deliver it to the busbars. The utilized solar cells were purchased from siliconsolar.com [32].

Comparing the solar cell surface with the PSD surface, as shown in Figure 1, one finds that the busbars of the front layer could be used as a cathode electrode, and the busbar at the back layer could be used as the common anode electrode. As a test, we measured the busbars output current signals while changing the laser beam position on the solar cell surface by using a digital multimeter. The result was not the same as that of the PSD. This result could be explained as follows.

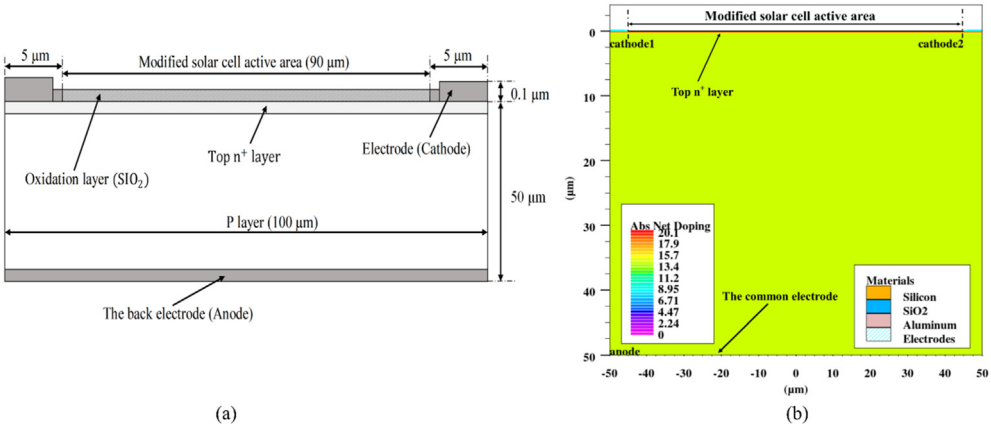

Figure 3. (a) The modified solar cell structure and (b) Schematic diagram of the modified solar cell simulation.

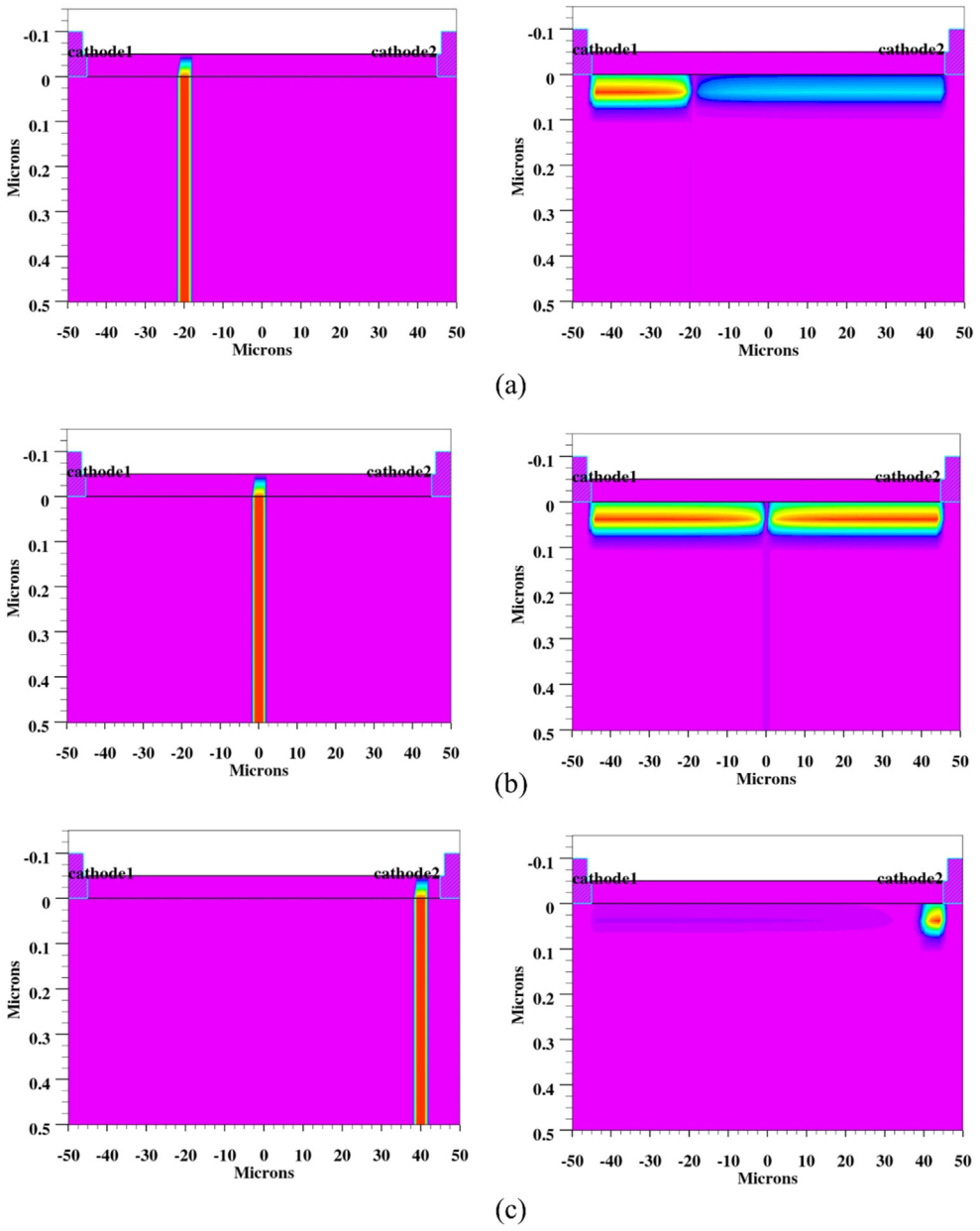

Figure 4. Modified solar cell sectional view showing the photogeneration rate (at the left) and the total current density (at the right) when the laser incident on different points: (a) at -20 μm from the center point, (b) center point and (c) at 40 μm from the center point.

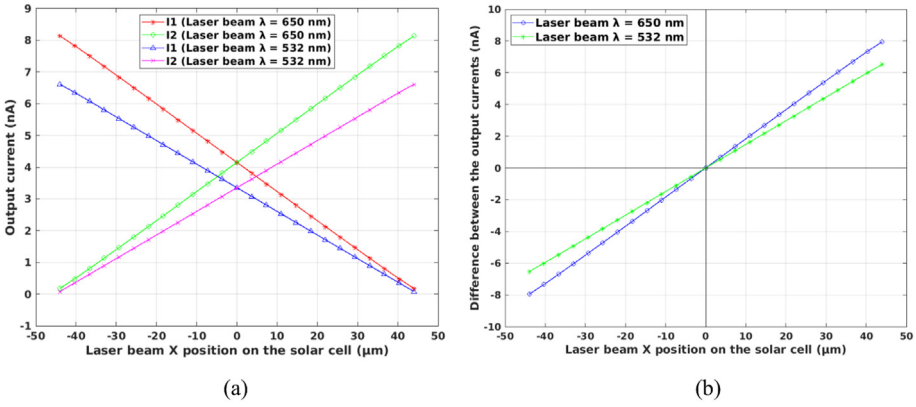

Figure 5. (a) The two output current signals while using two laser beams with different wavelength (b) The difference between the two output current signals.

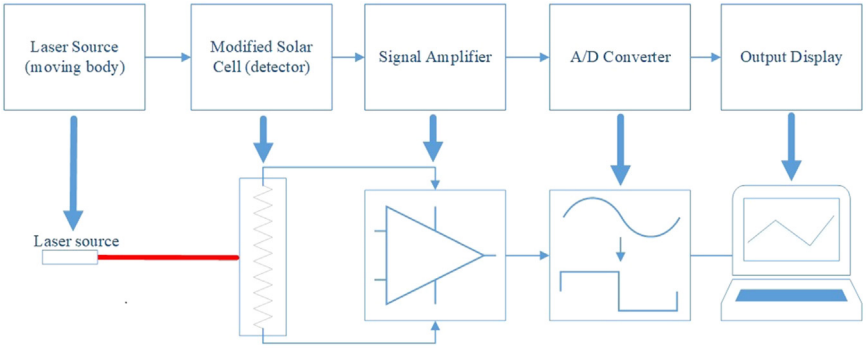

Figure 6. System block diagram.

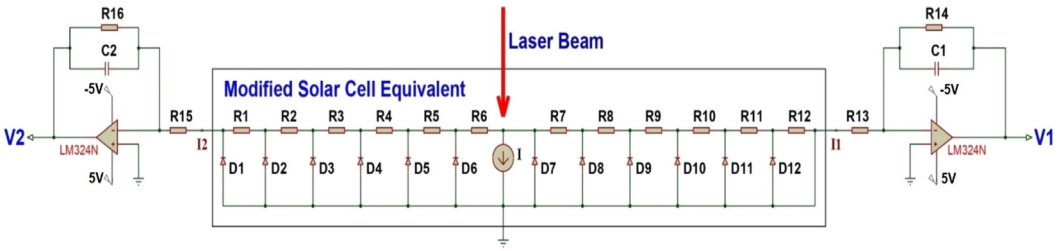

Figure 7. Equivalent circuit of the modified solar cell and the signal amplifier.

The fingers in the solar cells are thought to reduce the lateral resistance met by the photocurrent far away from the busbar. It is known that the series resistance reduces the fill factor of the solar cell and thereby reducing the power conversion efficiency of the solar cell. In the case of position sensitive detector, the solar cell structure is operated in short-circuit mode which renders the influence of the series resistance. So, the photocurrent generated in the solar cell will be a current source crossing the pn junction and it will be divided between the left and right electrodes according to the resistance seen in the top layer. If the fingers are not removed, they will collect the current early before it arrives to busbars of the end electrode. Here, it is required that the current must be forced to flow through the lateral resistance of the top layer.

Based on the previous discussion, a second experiment is performed to remove the fingers that connect the busbars to prevent the distribution of the output current between the busbars through them. Usually, solar cell fingers are made of silver, so using a chemical solution dedicated to silver etching would be the best option to disconnect the fingers due to the solar cell fragileness. A mixed solution of HNO_3:HCl:H_2O = 1:1:1 [33] was used. The solution components concentrations are: HNO_3 = 70% HNO_3 in H_2O and HCl = 37% HCl in H_2O.

The solar cell needs preparation before the etching process. First, tab wires are soldered to the bus bars (to read the output current signals from them later), then the cell is strengthened by fixing it on a board of plastic or glass, next the bus bars (the desired sensor electrodes) are masked using adhesive tape to protect them from the solution. After preparing the solar cell, it was entirely submerged in the solution from 3 to 4 h until the solution etches the fingers (depending on the solution concentration). After taking the cell out from the solution, it was rinsed with water and dried. Figure 9 shows a photograph of the cell after the etching process. The solar cell test was repeated after the chemical etching by using a digital multimeter and the result was as desired.

The elimination of silver fingers will affect the solar cell because it will increase the series resistance of the solar cell. While eliminating the silver fingers will impede the structure to function as an efficient solar cell device, it will empower its use as a large area position detector, as discussed herein. While etching the metal fingers, the other layers of the

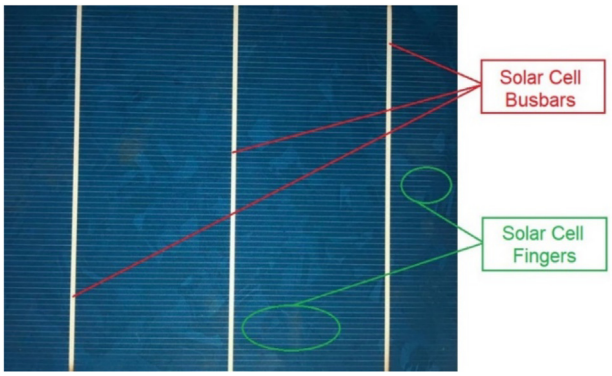

Figure 8. Image of a solar cell surface.

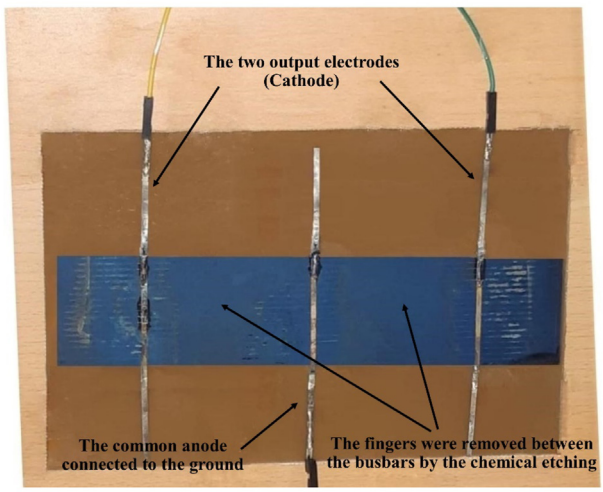

Figure 9. The modified solar cell.

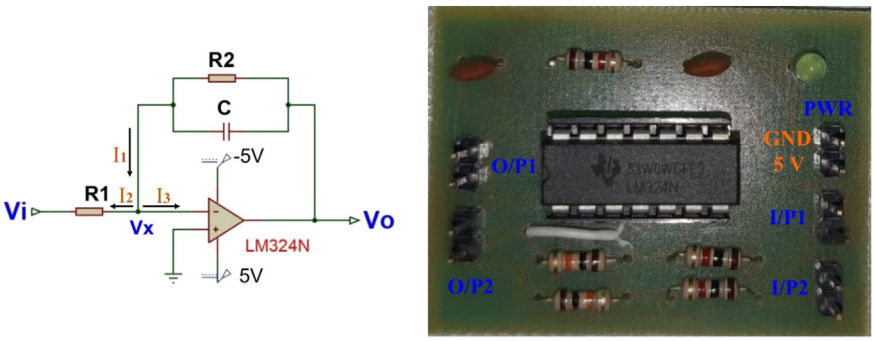

(a) (b)

Figure 10. (a) Inverting amplifier circuit by Proteus (b) Printed circuit board for the inverting amplifier circuit.

solar cells remain untouched. So, the layers required for the PSD are preserved after etching.

It should be pointed out here that if one wants to fabricate a PSD based on the solar cell structures as we proposed here, then it is preferred to pattern layers as that required for the PSD not for solar cell. In case of prototyping, we can modify the solar cell by etching the rest of the metallization layer except the edge busbars as we did here.

3.2.3. Signal amplifier

In this stage, the output signal needs to be amplified to make it readable in the next stage. As shown in Figure 10, the OP-AMP used is LM324N and the resistors are R1 = 1 kΩ and R2 = 10 kΩ. By a simple circuit analysis, we can find the gain is –10.

3.2.4. A/D converter

After amplifying the signal in the previous stage to a reasonable value, it has to be converted from analog to digital to transfer it to the computer in the next stage. Arduino Uno has been used in this stage as the microcontroller to read the analog signal and convert it into a digital signal. Then, the laser beam position on the sensor is calculated by the equation,

$$X = \frac{V_2 - V_1}{V_2 + V_1} * \frac{L}{2} \tag{4}$$

where L is the sensor active area length (resistance length), and the sensor origin is set at the sensor center.

3.2.5. Output display application

The final target of the whole system is to draw a path that represents the movement of the moving body. In order to illustrate that path using a PC, an application was developed by using C# Graphical User Interface (GUI) and ZedGraph class libraries. The application receives the data from the Arduino using serial communication, then it plots it.

Table 2. The Position detection error.

Actual Position (cm)	Measured Position (cm)	Error Percent (%)
1.3	1.19	8.46
2.5	2.3	8
3.2	3	6.25
4.65	4.45	4.3
-1.15	-1.06	-7.83
-2.8	-2.88	-2.86
-3.8	-3.76	-1.05
-4.7	-4.5	-4.25

3.3. Experimental results

After testing the system as shown in Figure 11, the experimental output results were taken from three signal paths that represent the two output voltage signals V_1, V_2 and the difference delta V between them at different laser positions on the modified solar cell surface. The results are depicted in Figure 12.

To evaluate the modified solar cell sensor behavior, the position error needs to be determined. The error, in this case, is a position detection error, which is the difference between the actual laser beam position on the solar cell surface and the measured position from the application. The position detection error percentage is calculated by using the following equation,

$$\Delta_p = \frac{x_L - x_{measured}}{x_L} \tag{5}$$

where Δ_P is the position detection error, x_L is the actual laser beam position on the solar cell and $x_{measured}$ is the measured position.

Table 2 illustrates te actual, measured and position error percentage for a set of measurements of some points. As shown in the table, the maximum percentage error is 8.5%, which does not exceed 10% and the mean percentage error is ±5.38%. The results are considered a proof of concept of using the modified solar cell as an efficient PSD.

It might be mentioned here that by comparing the modified solar cell and the commercial PSD [25], we can find the following differences. The resistance length of the modified solar cell is 100 mm while the largest available resistance length of the PSD in market is 37 mm. The position detection error for the PSD increases near the electrodes and decreases near the center, as for the modified solar cell it has the same trend. It has higher error near the electrodes and lower errors as the laser moves away

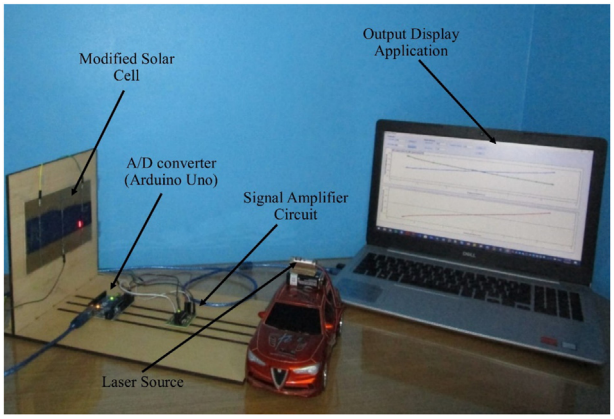

Figure 11. Photo of the practical system.

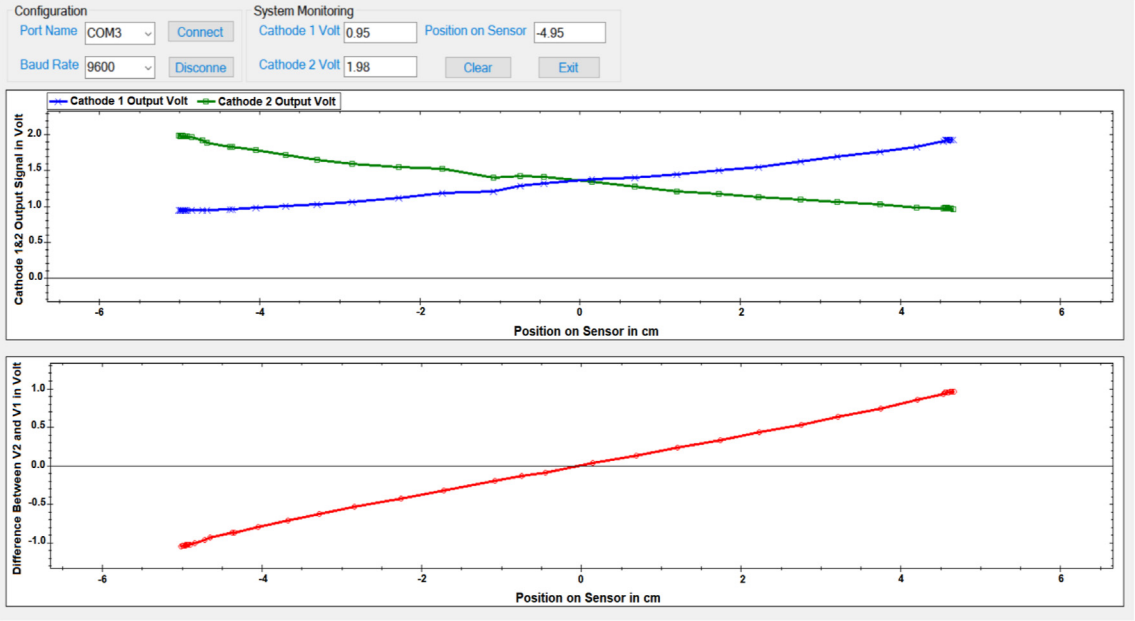

Figure 12. The experimental output results of the sensed voltages versus the laser beam position X. The upper waveform represents the two output voltage signals V_1, V_2 and the lower waveform represents the difference between them.

from them. The output signals from both the PSD and modified solar cell have a linear relation because of the uniform resistivity of the surface layer of both.

3.4. Limitations and suggestions for the proposed system

The main drawback of the proposed technique, in this current work, is that the developed sensor is only applicable for a one-dimensional motion. The reason is that the solar cell available for us was constructed to have only two major edge busbars and then we could only collect the current from the left and the right edges where the busbars. So, the dimensionality of our PSD was restricted by the original metallization pattern of the available solar cells. For the two-dimensional PSD, one must have two sets of edge electrodes one set is horizontal and the other set is vertical. Besides, the method could be extended for three-dimensional detection by evaluating the received signal relative to the sent signal.

Other possible limitations of our work are listed as follows. The laser beam must not be obstructed in its way to the sensor. So, it must not be scattered by the surrounding. Further, only one laser beam can be detected at any time. So, in the case of multiple beams, one must distinguish them from each other by modulating the laser beam with specific tones. Moreover, the background light could affect the reading; however, this issue may be solved by calibrating the system before reading or by using an optical filter. We believe that more investigations are needed to extend the capabilities of this promising low-cost position sensitive detector.

4. Conclusion

This paper presented how the solar cell could be modified to work as a PSD. We also illustrated how to make a motion detection system consisting of the modified solar cell, a simple processing circuit and a computer application to display the path that represents the moving body position. This system has many qualifications such as its low cost compared to other systems, where the cost of the solar cell plus the other components were approximately 6.5$ + 10$, so the total system cost is less than 20$. Moreover, the system has a moderate accuracy since the maximum position detection error is ±8.5%. Besides, the system has a high-speed response that can be controlled by changing the delay time in the application code, and for the detection and tracking of a moving body in a large area, which could be achieved by using multiple of modified solar cells. Our future work will focus to develop a very large area 2D PSD using two-dimensional solar cell arrays.

Declarations

Author contribution statement

Heba Abdelmoneim, Abdelhalim Zekry & Ahmed Shaker: Conceived and designed the experiments; Performed the experiments; Analyzed and interpreted the data; Contributed reagents, materials, analysis tools or data; Wrote the paper.

Funding statement

This research did not receive any specific grant from funding agencies in the public, commercial, or not-for-profit sectors.

Data availability statement

Data will be made available on request.

Declaration of interests statement

The authors declare no conflict of interest.

Additional information

No additional information is available for this paper.

References

[1] A. Senior, An introduction to automatic video surveillance, in: Protecting Privacy in Video Surveillance, Springer, London, 2009, pp. 1–9.
[2] H. Zhou, H. Hu, Human motion tracking for rehabilitation—a survey, Biomed. Signal Process Contr. 3 (1) (2008) 1–18.
[3] B. Pueo, J.M. Jimenez-Olmedo, Application of motion capture technology for sport performance analysis, Retos 2041 (32) (2017) 241–247.
[4] J.V. Condell, G. Moore, J. Moore, Software and methods for motion capture and tracking in animation, in: CGVR, 2006, pp. 3–9.
[5] E. Fortunato, G. Lavareda, M. Vieira, R. Martins, Thin film position sensitive detector based on amorphous silicon p–i–n diode, Rev. Sci. Instrum. 65 (12) (1994) 3784–3786.
[6] M. Vieira, Speed photodetectors based on amorphous and microcrystalline silicon p–i–n devices, Appl. Phys. Lett. 70 (2) (1997) 220–222.
[7] V. Jaiswal, V. Sharma, S. Varma, Comparative analysis of CCTV video image processing techniques and application: a survey, IOSR J. Eng. (2018) 38–47.
[8] A. Kailas, Basic human motion tracking using a pair of gyro+ accelerometer MEMS devices, in: 2012 IEEE 14th International Conference on e-Health Networking, Applications and Services (Healthcom), IEEE, 2012, pp. 298–302.
[9] J.Y. Lee, K.B. Lee, S.H. Choi, A design of motion detecting sensor using microwave, in: 2007 Asia-Pacific Microwave Conference, IEEE, 2007, pp. 1–4.
[10] R. Canals, P. Ying, T. Deschamps, J. Zisa, Pedestrian detection and localization system by a new multi-beam passive infrared sensor, in: International Conference on Indoor Positioning and Indoor Navigation 28, 2013, p. 31.
[11] C.J. Borkowski, M.K. Kopp, Some applications and properties of one-and two-dimensional position-sensitive proportional counters, IEEE Trans. Nucl. Sci. 17 (3) (1970) 340–349.
[12] C. Li, Z. Tang, G. Lin, Z. Li, J. Jia, Rotational speed measurement using one-dimensional position sensitive detector, in: 2016 IEEE Advanced Information Management, Communicates, Electronic and Automation Control Conference (IMCEC), IEEE, 2016, pp. 1499–1502.
[13] A. Cerezo, T.J. Godfrey, G.D.W. Smith, Application of a position-sensitive detector to atom probe microanalysis, Rev. Sci. Instrum. 59 (6) (1988) 862–866.
[14] I.A. Ivan, M. Ardeleanu, G.J. Laurent, N. Tan, C. Clevy, The metrology and applications of PSD (position sensitive detector) sensors for microrobotics, in: 2012 International Symposium on Optomechatronic Technologies (ISOT 2012), IEEE, 2012, pp. 1–2.
[15] X. Qiang, Y. Li, F. Zong, J. Zhao, Measurement of laboratory-simulated atmospheric turbulence by PSD, in: 2009 9th International Conference on Electronic Measurement & Instruments, IEEE, 2009, pp. 2–90.
[16] S. Das, A. Saha, Laser beam position-dependent PSD-based calibrated self-vibration compensated noncontact vibration measurement system, IEEE Trans. Instrum. Meas. 68 (9) (2018) 3308–3320.
[17] H.M. Adel, A. Zekry, N. AbdRabou, Development of large area motion tracking system, in: 2019 7th International Japan-Africa Conference on Electronics, Communications, and Computations, (JAC-ECC), IEEE, 2019, pp. 101–105.
[18] TCAD - silvaco. https://silvaco.com/tcad/.
[19] A. Zekry, A. Shaker, M. Salem, Solar cells and arrays: principles, analysis, and design, in: Advances in Renewable Energies and Power Technologies, Elsevier, 2018, pp. 3–56.
[20] M.S. Salem, A. Zekry, A. Shaker, M. Abouelatta, T.M. Abdolkader, Performance enhancement of a proposed solar cell microstructure based on heavily doped silicon wafers, Semicond. Sci. Technol. 34 (3) (2019), 035012.
[21] J. Sharp, Microsoft Visual C# Step by Step, ninth ed., Pearson Education, Inc, 2018.
[22] ZedGraph. https://sourceforge.net/projects/zedgraph/.
[23] G. Lucovsky, Photoeffects in nonuniformly irradiated p-n junctions, J. Appl. Phys. 31 (6) (1960) 1088–1095.
[24] I. Chen, A theoretical model of lateral photoeffects in amorphous materials, J. Appl. Phys. 64 (4) (1988) 2224–2226.
[25] Hamamatsu Photonics K.K, Solid State Division, PSD (POSITION SENSITIVE DETECTOR), 2002.
[26] A. Arefin, K. Tul Kubra Prianka, M. Billal Hosain, A. Haque Snigdha, Characterization and Analysis of Quantum-Dot PV Solar-Cells, 2016.
[27] D.K. Gupta, M. Langelaar, M. Barink, F. van Keulen, Optimizing front metallization patterns: efficiency with aesthetics in free-form solar cells, Renew. Energy 86 (2016) 1332–1339.
[28] A. Fantoni, M. Vieira, J. Cruz, R. Schwarz, R. Martins, A two-dimensional numerical simulation of a non-uniformly illuminated amorphous silicon solar cell, J. Phys. Appl. Phys. 29 (12) (1996) 3154–3159.
[29] PCB design and circuit simulator software - Proteus. https://www.labcenter.com/.
[30] A. Zekry, A.Y. Al-Mazroo, A distributed SPICE-model of a solar cell, IEEE Trans. Electron. Dev. 43 (5) (1996) 691–700.
[31] K.F. Renk, Basics of Laser Physics, Springer Berlin Heidelberg, Berlin, 2012.
[32] 45 watt DIY educational solar panel kits. https://www.siliconsolar.com/product/build-your-own-45w-diy-solar-panel/.
[33] MicroChemicals, Wet-chemical etching of metals. https://www.microchemicals.com/technical_information/wet_etching_metals_al_au_cu_cr_ni_ti_ag.pdf.